Facile Synthesis of TiO$_2$−SiO$_2$−P$_2$O$_5$/CaO/ZnO with a Core−Shell Structure for Bone Implantation

Ekaterina S. Lyutova, Valeriya A. Tkachuk, Liliya A. Selyunina, Lyudmila P. Borilo, Dmitriy A. Fedorishin, and Yu-Wen Chen*

Read Online

ACCESS | Metrics & More | Article Recommendations

ABSTRACT: A facile synthesis method was developed to synthesize TiO$_2$−SiO$_2$−P$_2$O$_5$/CaO or TiO$_2$−SiO$_2$−P$_2$O$_5$/ZnO with a core−shell structure. The carboxylic cation exchanger Tokem-250 has a high selectivity for Ca^{2+}/Zn^{2+} ions and was used in this study. The framework of the material in the shell was TiO$_2$−SiO$_2$−P$_2$O$_5$, and the inner part was filled with CaO (sample TiO$_2$−SiO$_2$/CaO) or ZnO (sample TiO$_2$−SiO$_2$−P$_2$O$_5$/ZnO). A stepwise heat treatment (drying in a drying oven at 60 °C for 30 min, then annealing in a muffle furnace for 30 min at 150, 250, and 350 °C, at 600 °C for 6 h, and at 800 °C for 1 h) was needed to obtain a homogeneous material. The poly(vinyl alcohol) was used as a binding additive. The obtained composites were characterized by a regular structure and highly developed surface. The samples exhibit bioactive properties in the simulated body fluid (SBF) solution, since the surface contains active centers (Si^{4+}, Ti^{4+}) which contribute to mineralization and precipitation of the calcium-phosphate compounds on the surface from biological media. The TiO$_2$−SiO$_2$−P$_2$O$_5$/CaO-PVA samples did not exceed acceptable hemolysis levels for medical materials.
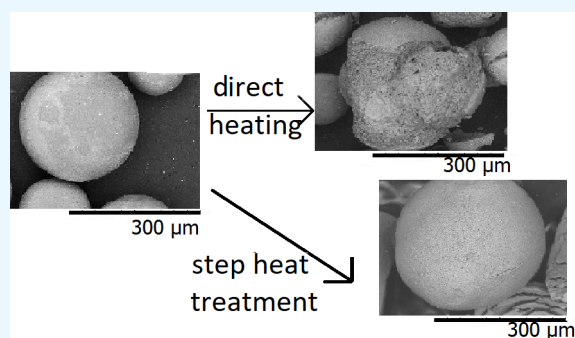
1. INTRODUCTION

Bone is a natural composite, which contains about 60 wt % minerals, 30 wt % matrix, and 10 wt % water.[1] Injuries and bone defects occur regularly, and each time a bone is fractured, it needs surgery with the use of an implantable material that can carry the load of the entire body. Traditional metallic materials such as stainless steel and alloy based on titanium are used in medical treatment. However, these materials are bioinert; i.e., they are not capable of forming a layer on their surface for fusion with natural bone.[2−4]

In addition, such materials must have a number of specific properties, such as adgesis, strength, and ability to withstand the high stresses to which bone tissue is subjected. In addition, the material must not have a toxic effect on the human body.[5−7] One of the most traditional and widespread methods of increasing the biocompatibility and bioactivity of the material is to cover the surface with a film of a special composition.[8−11]

Bioactive glasses are highly biocompatible and are more likely to integrate with human tissue than metal implants. This makes them a good alternative for improving biocompatibility when placed on a metal substrate.[12] The addition of compounds contained in bone tissue to such glasses allows increasing the bioactive properties of the materials. Such compounds can be various calcium[13] and phosphorus compounds.[14−16] Tricalcium phosphate belong to the group

of biologically active synthetic materials due to its osteoconductivity, crystallographic structure and ability to form chemical bonds with living bone tissues.[17,18] Therefore, the development of various modified calcium-phosphate materials is needed for regenerative medicine. It is noted that the introduction of organic and inorganic modifying compounds in their composition improves the biological characteristics of calcium-phosphate materials.[17]

In recent years, materials with zinc oxide additives have attracted the attention of researchers, as they have great potential in orthopedic applications.[18,19] Zinc plays an important role in bone formation. It participates in various metabolic processes and activates proteins involved in bone homeostasis.[20] Zinc oxide accelerates bone growth and mineralization, and it is also known to be toxic to bacteria.[21,22] At the same time, it has low toxicity, high chemical stability, and biological activity and compatibility with bone tissue.[23] A reduction in zinc levels impairs bone growth.[24−29] In recent years, spherical polymeric composites have been used to fill

bone defects. They act as a biodegradable framework. New bone tissue would be formed on it.[30] In the process of decomposition, simple substances are formed that are easily excreted from the body.[31] There are many methods of obtaining such materials. But the most promising is the sol−gel technology. It allows one to obtain materials with different compositions, uniform distribution of phases in multicomponent system, and with a given particle size.[32] The use of the sol−gel method allows one to control the size of particles forming spheres based on titanium and silicon oxides, which preserves the porosity of the material and ensures access of physiological fluids to the entire volume of bone tissue. Such materials can be used in the production of implants and regenerative medical materials with the required biological properties. Packaging the spheres into the required shape using polymeric binding additives would make it possible to produce implants of a new quality. Medical and orthopedic centers can become consumers of such materials. Composites with a core−shell structure in recent years in medicine are widely used to fill bone defects, but the influence of compositions and preparation conditions on the structure and properties of composites has not been studied in detail.

The aim of this work was to investigate the influence of the compositions and preparation conditions on the structure and the properties of composite materials $TiO_2-SiO_2-P_2O_5/CaO/ZnO$ with a spherical shape of particles using the cationic exchange resin Tokem-250 in preparation.

2. EXPERIMENTAL SECTION

2.1. Chemicals. Tetraethoxysilane (Puriss. Spec., Germany), orthophosphoric acid (Puriss. spec. Himmed Russia), calcium nitrate (p. a. Himmed Russia), zinc nitrate (p. a. Himmed Russia), and tetrabutoxytitanium (puriss. spec. Germany), and butyl alcohol were used as received from vendors.

2.2. Synthesis of Materials. The outer framework, the obtained materials were $TiO_2-SiO_2-P_2O_5$, and the inner part was filled with CaO (sample $TiO_2-SiO_2-P_2O_5/CaO$) or with ZnO ($TiO_2-SiO_2-P_2O_5/ZnO$). The calcium-containing/zinc-containing samples of acryl-divinylbenzene-based Tokem-250 cationite were chosen due to their high selectivity for Ca^{2+}/Zn^{2+}. An aggregation stable sol was prepared to form a $TiO_2-SiO_2-P_2O_5$ framework.[33,34] Composition of aggregation stable sol in terms of oxides: TiO_2 (65 mol %)−SiO_2 (30 mol %)−P_2O_5 (5 mol %).

Tokem-250 samples with Ca^{2+}/Zn^{2+} were immersed in the aggregation stable sol for 12 h, followed by extraction and drying in a drying oven at 60 °C for 60 min. After drying, the samples were annealed in a muffle furnace for 30 min at 150, 250, 350 °C, for 6 h at 600 °C, and for 1 h at 800 °C.

Introduction of binder additives was as follows: PVA in a 1:1 ratio was added to the dried samples of Tokem-250 with Ca^{2+}/Zn^{2+} and the applied sol, and then the specimens were frozen.

2.3. Characterization. The sample was dried at 60 °C before testing. It was studied with a synchronous thermal analyzer STA 449 C Jupiter in an oxygen atmosphere following the shape of TG and DSK curves in the temperature range between 60 and 1000 °C.

IR spectra of the samples were taken on a Nicolet 6700 FTIR spectrometer in the frequency range of 400−4000 cm^{-1}.

The surface morphology of the samples was examined on a TM-3000 scanning electron microscope (SEM) (Hitachi, Japan) with an accelerating voltage of 15 kV (electron gun 5

× 10^{-2} Pa, camera for the sample 30−50 Pa). X-ray microanalysis was performed on the Quanax-70 console using energy dispersive X-ray.

2.4. Biomimetic Properties. Biomimetic properties of the materials under artificial conditions were determined in SBF (simulated body fluid) solution. The samples were immersed in the SBF solution for 14 days at 37 °C with daily updating of the solution.

To determine the rate of formation of calcium-phosphate layer on the surface of the materials, the total concentration of calcium and magnesium ions (C (Ca^{2+} and Mg^{2+}), mmol/L) was measured in SBF solution by trinometric titration. Accumulation coefficient of Ca^{2+} and Mg^{2+} ions, was calculated by the formula

$$k = \frac{C(Ca^{2+} \text{and} \, Mg^{2+})}{\tau}$$

where M mol/L is the total change in concentration during the time interval τ (day).

The whole hemostatic blood from a healthy donor was used to evaluate the hemocompatibility of the samples. The blood was centrifuged and the erythromass was separated. The resulting erythromass was diluted with sterile 1× PBS solution at 37 °C at a ratio of 1:9. Samples were placed in a standard 24-well cell culture plate and filled with the resulting blood solution in PBS at a ratio of 1 mL of solution per 1 cm^2 of sample surface area. Deionized water was used as a negative control, and a 1× PBS solution was used as a positive control. The hemolysis level of the negative control was taken as 100% hemolysis, and the hemolysis level of the positive control was taken as 0% hemolysis. Then the plate was incubated in an incubator at 37 °C for 60 min. After that the blood was transferred from the plate wells to centrifuge tubes and centrifuged for 5 min at 3000 rpm to precipitate the remaining erythrocytes. The supernatant was then carefully removed and transferred to a standard 96-well plate for spectroscopic analysis at 545 nm and analyzed using a Tecan Infinite F50 ELISA reader (Tecan Inc., USA). The percentage of hemolysis was the average of three replicates and was calculated using the following equation:

$$\text{hemolysis} = \frac{OD_{test} - OD_{control}^{negative}}{OD_{control}^{positive} - OD_{control}^{negative}} \times 100\%$$

3. RESULTS AND DISCUSSION

3.1. Sorption Properties of Cationic Exchange Resins. The choice of cationic exchange resins for obtaining materials

Table 1. Physical and Chemical Properties of Tokem-250 Cationic Exchange Resins

cation	total exchange capacity (mmol/g)	sorption capacity (mmol/g)	humidity (%)
Ca^{2+}	10.25 ± 0.27	8.60 ± 0.08	54.0 ± 0.5
Zn^{2+}	10.25 ± 0.27	7.55 ± 0.08	54.0 ± 0.5

with a spherical shape of particles was based on the results of studies of physical and chemical properties of cationic exchange resins Tokem-250 and their selectivity for Ca^{2+}/Zn^{2+} ions (Table 1).
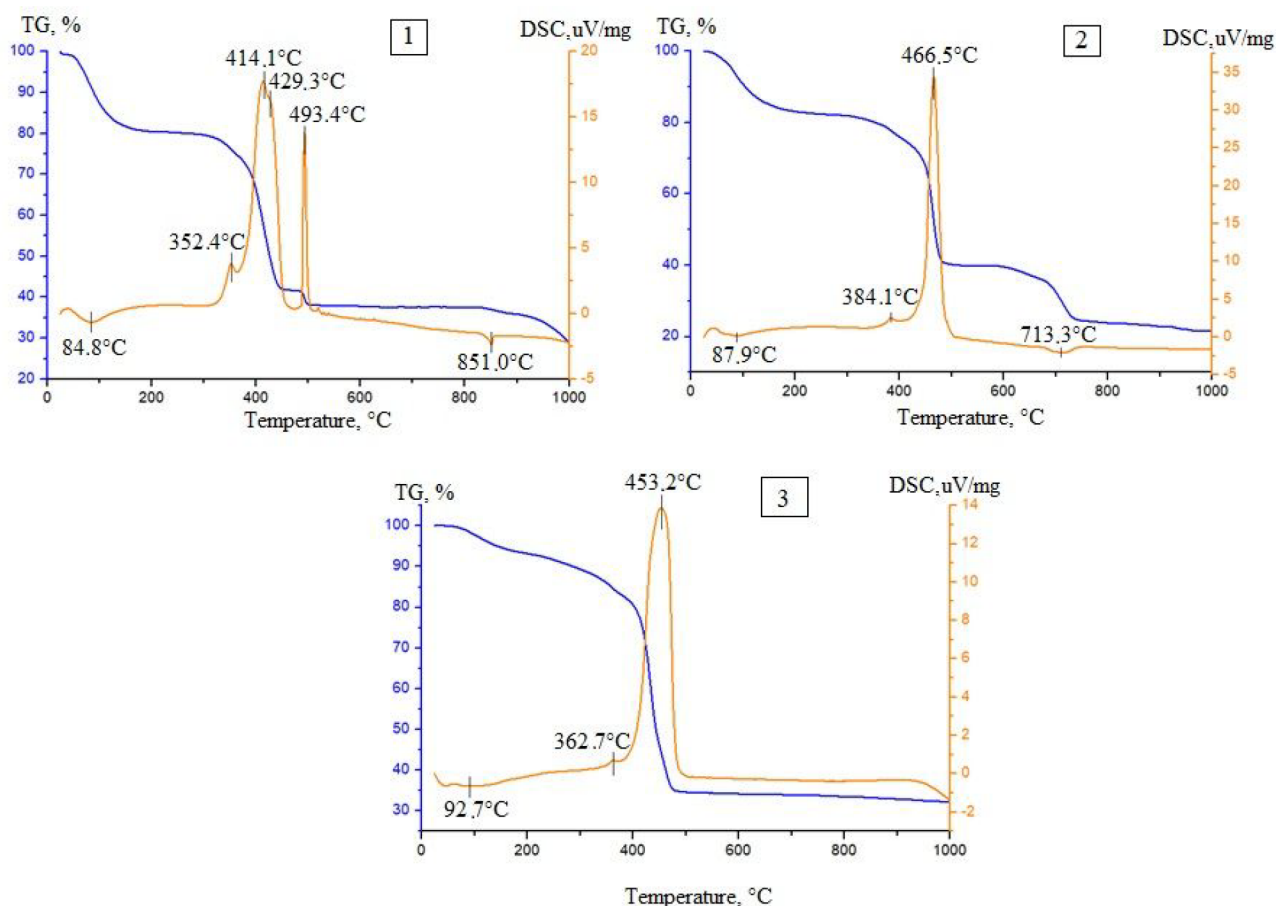
Figure 1. Thermogravimetric analysis of the samples: Tokem-250 (1), $TiO_2-SiO_2-P_2O_5/CaO$ (2), and $TiO_2-SiO_2-P_2O_5/ZnO$ (3).
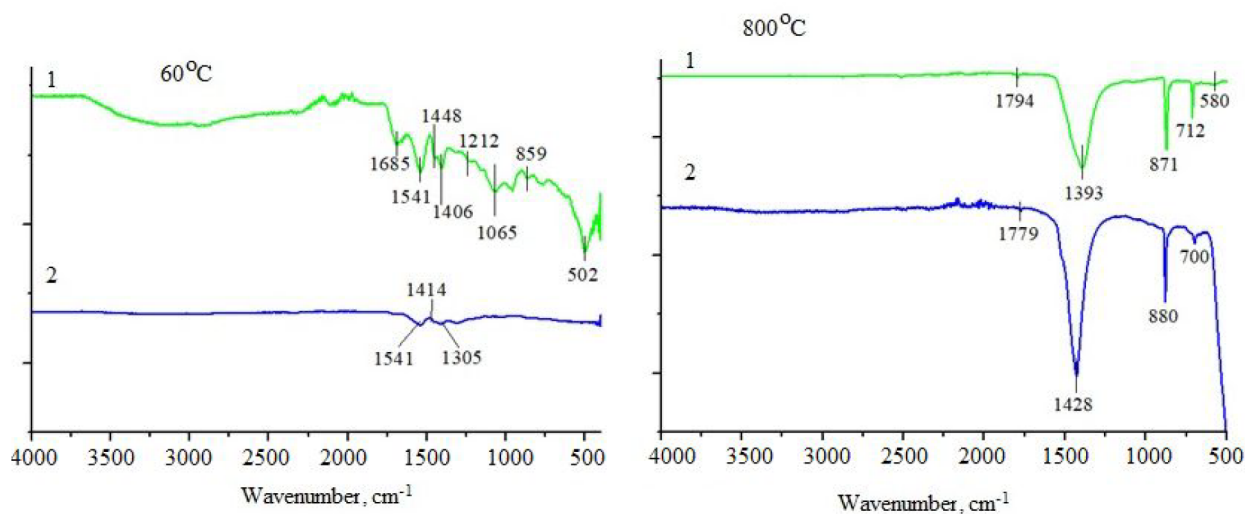
Figure 2. Infrared spectra of the samples. (1) $TiO_2-SiO_2-P_2O_5/CaO$; (2) $TiO_2-SiO_2-P_2O_5/ZnO$.

The results of total exchange capacity, sorption capacity, and humidity indicate that most of the functional groups of the cationic exchange resin were involved in the sorption process.

3.2. Thermogravimetric Analysis and IR Spectroscopy. The temperature modes and stages of formation of $TiO_2-SiO_2-P_2O_5/CaO$ and $TiO_2-SiO_2-P_2O_5/ZnO$ samples were determined by thermal analysis (Figure 1). Up to 400 °C (Figure 1.1), removal of physically and chemically bound water

and combustion of cationic exchange occurred. The second stage, between 400 and 600 °C, is characterized by the removal of the organic matrix of Tokem-250 cationite. As a result, the cationite structure was destroyed. For samples $TiO_2-SiO_2-P_2O_5/CaO$ (Figure 1.2) and $TiO_2-SiO_2-P_2O_5/ZnO$ (Figure 1.3) at the temperature range from 400 to 600 °C, removal of the organic matrix continues and decomposition of zinc and calcium nitrates occurred. For the sample $TiO_2-SiO_2-P_2O_5/$
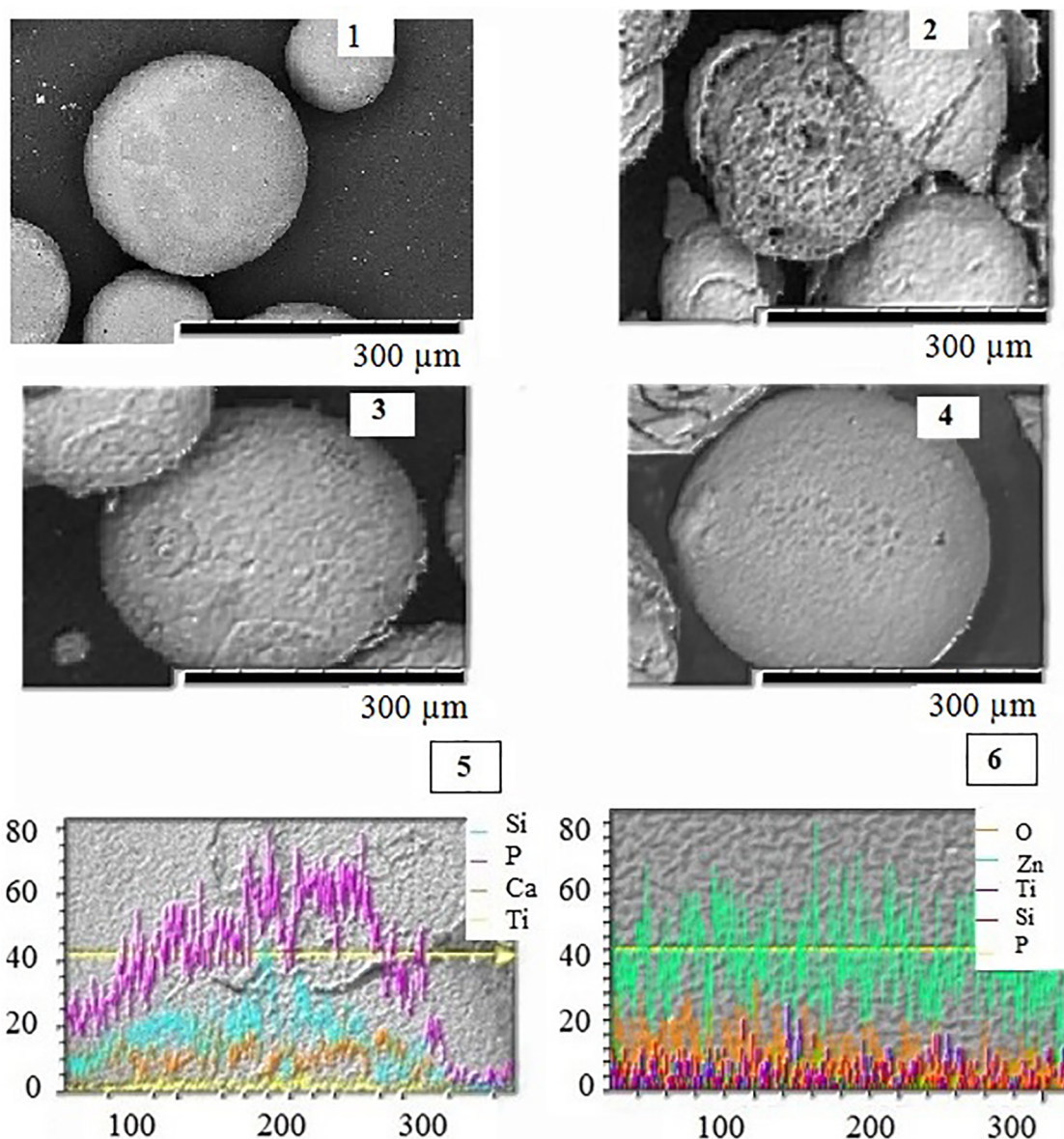
Figure 3. Microphotographs and distribution of the elements on the surface of the samples. (1) Tokem-250, (2) 800 °C annealing; (3, 4) step heat treatment; (3, 5) $TiO_2-SiO_2-P_2O_5/CaO$; (4, 6) $TiO_2-SiO_2-P_2O_5/ZnO$.
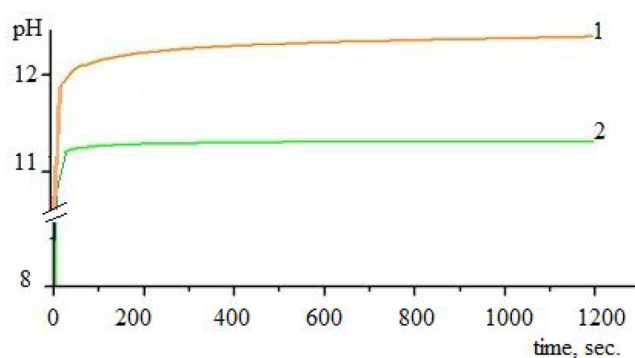
Figure 4. Kinetic curves of pH changes in aqueous suspensions. (1) $TiO_2-SiO_2-P_2O_5/CaO$; (2) $TiO_2-SiO_2-P_2O_5/ZnO$.

CaO at the temperature range from 600 to 800 °C, the transition of amorphous modifications of compounds into crystalline ones was observed.

IR spectroscopy results (Figure 2) of the samples dried at 60 °C and annealed at 800 °C confirm the results of the thermal analysis.

For the sample treated at a temperature of 60 °C, absorption bands in the range of 3265−3475 and 1305−1310 cm^{-1} were observed, which correspond to the valence and stretching vibrations of OH, respectively. The absorption bands in the range of 2849−3920 cm^{-1} correspond to the valence vibrations of C−H. After annealing at 800 °C, absorption bands in the range of 1395−1428 and 680−886 cm^{-1} appeared and they corresponded to the valence vibrations of Ti−O(H)-Ti, δ(Si−O−Si). The absorption bands in the range 700−702 cm^{-1} correspond to the valence vibrations of Ti−O of the TiO$_4$ tetrahedron. The 880 cm^{-1} absorption band characteristic of
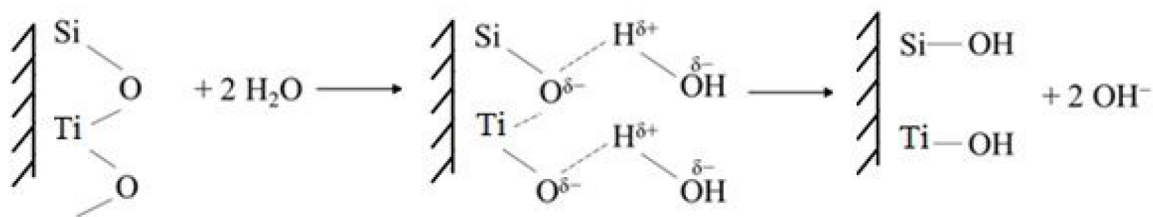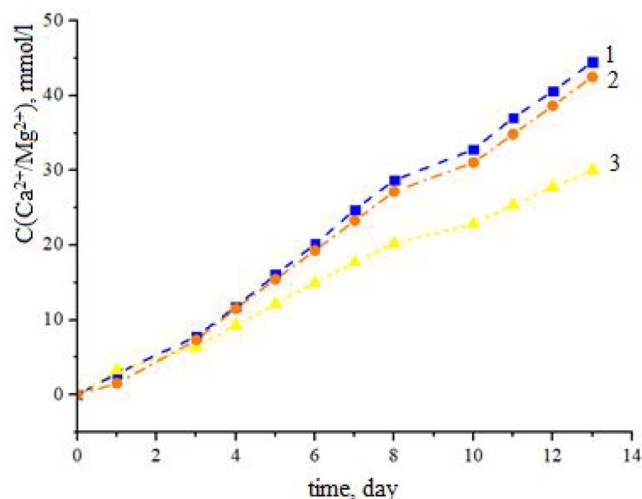
Figure 5. Scheme of the adsorption mechanism.

Figure 6. Curves of Ca^{2+} and Mg^{2+} ion accumulation on the material surface. (1) $TiO_2-SiO_2-P_2O_5/ZnO$; (2) $TiO_2-SiO_2-P_2O_5/CaO$:-$TiO_2-SiO_2-P_2O_5/ZnO = 1:1$; (3) $TiO_2-SiO_2-P_2O_5/CaO$.

Table 2. Coefficient of Ca^{2+} and Mg^{2+} Ion Accumulation on the Material Surface

sample	k (0–3 cyr.)	k (4–8 cyr.)	k (9–14 cyr.)
$TiO_2-SiO_2-P_2O_5/Ca$	1.62	1.28	0.87
$TiO_2-SiO_2-P_2O_5/Zn$	1.78	1.73	1.22
$TiO_2-SiO_2-P_2O_5/Ca$:TiO_2- $SiO_2-P_2O_5/Zn = 1:1$	1.48	1.66	1.21

stretching vibrations of ZnO is also recorded for this system. The absorption bands in the 445–472 cm^{-1} region are fixed

for the $TiO_2-SiO_2-P_2O_5/CaO$ system and correspond to the Ca−O vibrations in $[CaO_6]$.

3.3. Microstructure. Figure 3 shows microphotographs of the samples. It was found that the samples without step treatment (drying 60 °C and annealing 800 °C) (Figure 3.2) did not retain the spherical shape and had cracks on their surface. It is not favorable for practical applications. A stepwise heat treatment is necessary to completely remove the carbon and preserve the spherical shape of the composite. Drying in a drying oven at 60 °C for 30 min, then annealing in a muffle furnace for 30 min at 150, 250, 350 °C, for 6 h at 600 °C and for 1 h at 800 °C is necessary (Figure 3.3 and 4). Thermal treatment leads to the formation of mesoporous materials with a highly developed surface, which is necessary for fixing biological cells when introducing the sample into the biological media. Figure 3.5 and 6 shows that after the step-by-step treatment, the elements are uniformly distributed on the surface of the samples.

3.4. Acid−Base Properties. The acid−base properties on the surface of the samples annealed at 800 °C were studied to determine the surface charge of the material (Figure 4). The surface charge affects the distribution of ions around it when it is immersed in the SBF.

It was found that during the first 10 s the desorption of the hydroxyl-hydrate occurred, with a sharp increase in the pH value of the suspension. After 16 min, the pH value stabilized in the range between 11.2 and 12.5, indicating that the surface of the samples was basic. With Si−OH, Ti−OH bonds were not identified in the samples calcined at 800 °C, as shown in the IR spectra. The surface contained the Lewis basic sites. While in the solution, the samples interacted with the protons of water molecules by their basic sites. The OH⁻ groups of water became less firmly bound and passed into solution. This
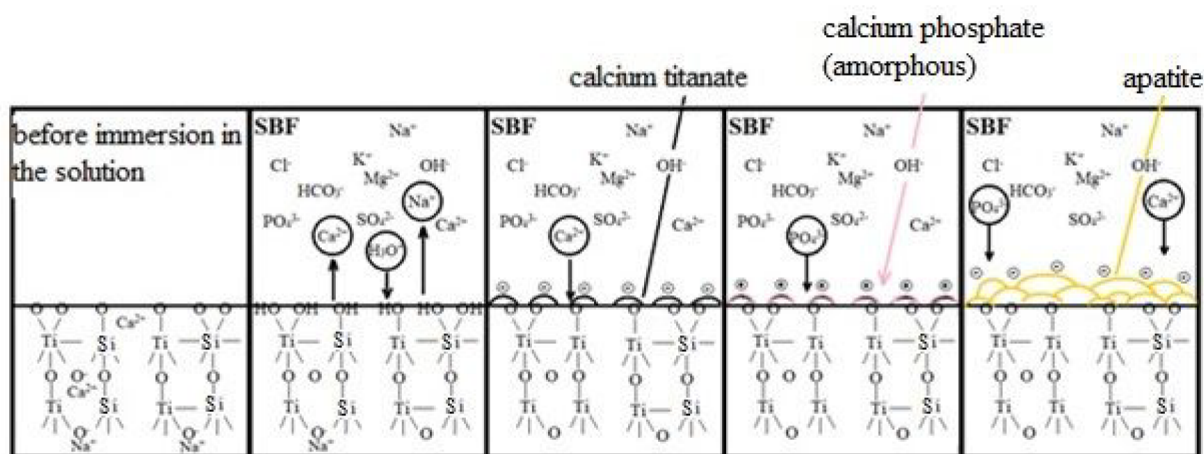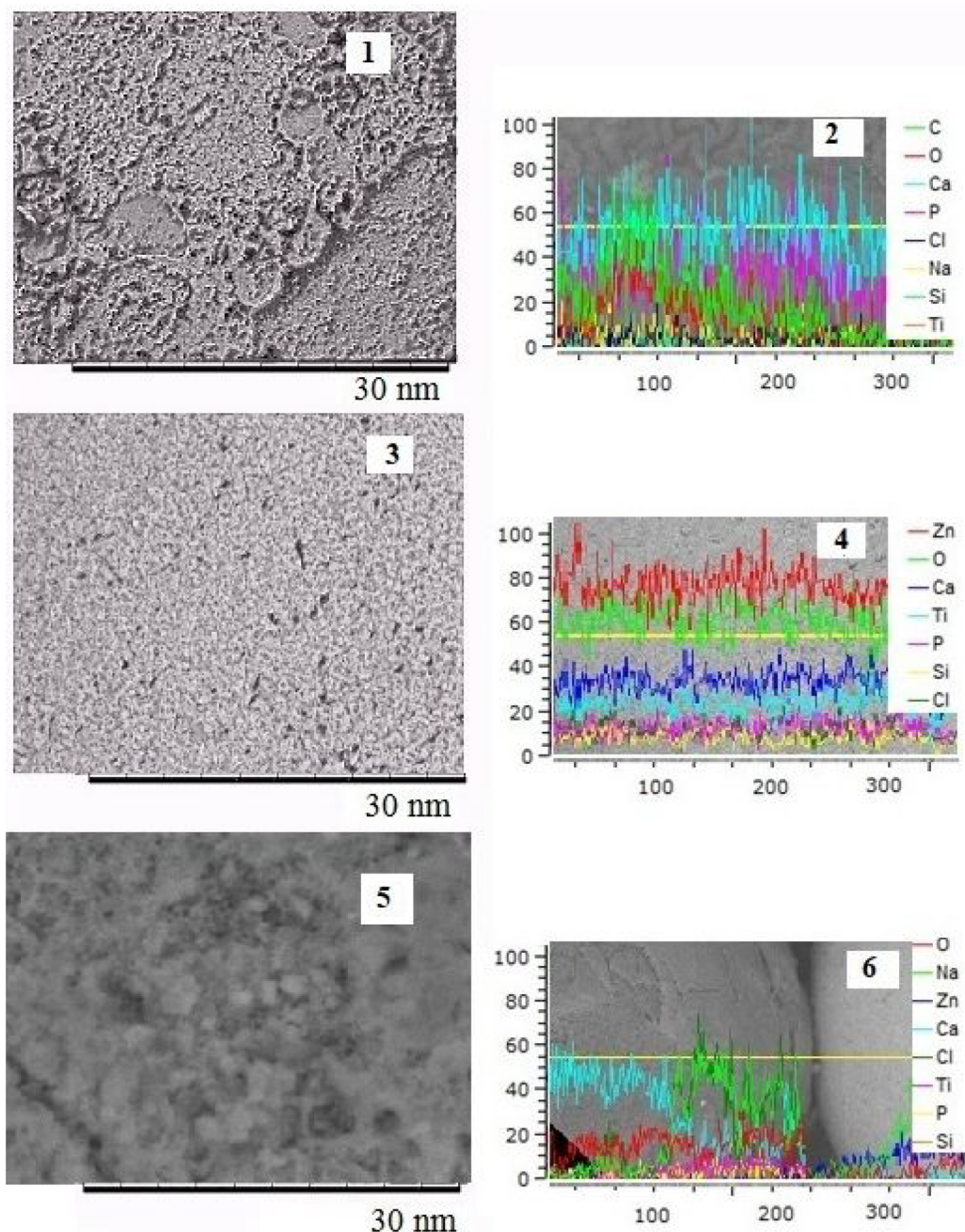

Figure 7. Mechanism of apatite-like layer formation on the surface of the samples.

Figure 8. Microphotographs of samples and distribution of elements by line after immersion in SBF solution for 14 days: 1, 4 - $TiO_2-SiO_2-P_2O_5/CaO$; 2, 5 - $TiO_2-SiO_2-P_2O_5/ZnO$; 3, 6 - $TiO_2-SiO_2-P_2O_5/CaO:TiO_2-SiO_2-P_2O_5/ZnO = 1:1$.

leads to a sharp increase in the basicity of the medium. Lewis basic sites turned to Bronsted basic sites. The scheme of the mechanism is shown in Figure 5.

3.5. Biomimetic Properties. The samples were immersed in a model SBF solution to determine the effect of zinc oxide on the ability of the materials to form a calcium-phosphate layer on the surface. Figure 6 shows the curves of Ca^{2+} and Mg^{2+} ion accumulation on the sample surface adsorbed from SBF solution. It shows that the deposition of ions occurred in three stages, the coefficient of ion accumulation on the material surface in each stage was calculated and listed in Table 2.

The sedimentation occurred at a high rate in the first 3 days (the coefficient of accumulation has values in the range of 1.48−1.78). This can be explained by the migration of alkaline

and alkaline earth elements, due to the formation of hydroxyl groups on the surface of the samples. After 4 days of the accumulation of Ca^{2+} and Mg^{2+} ions and the formation of an amorphous layer on the surface of the samples, the deposition rate decreased (the accumulation coefficient has values from 1.28 to 1.73). After 9 days, the stabilization of ions deposition on the surface of samples began (the coefficient of accumulation is in the range of 0.87−1.22). It was found that the accumulation of Ca^{2+} and Mg^{2+} ions was faster on the $TiO_2-SiO_2-P_2O_5/Zn$ sample, which indicates a higher ability to form a calcium-phosphate layer on the surface in the SBF model solution. When the samples were immersed in SBF solution, the pH of the medium increased significantly from 7.4 to 8.4 during the first day. After that, the pH increased
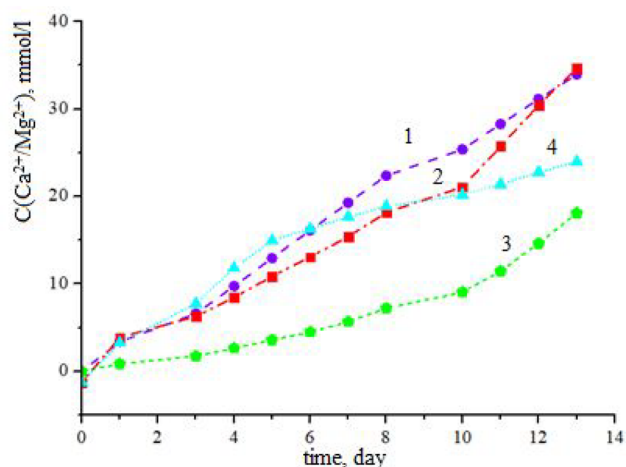
Figure 9. Curves of Ca^{2+} and Mg^{2+} ion accumulation on the material surface: (1) $TiO_2-SiO_2-P_2O_5/CaO\_PVA$; (2) $TiO_2-SiO_2-P_2O_5/ZnO\_PVA$; (3) $TiO_2-SiO_2-P_2O_5/CaO:TiO_2-SiO_2-P_2O_5/ZnO\_P-VA = 1:1$; (4) Tokem-250_PVA.

Table 3. Coefficient of Ca^{2+} and Mg^{2+} Ions Accumulation on the Material Surface

sample	k (0−3 days)	k (4−8 days)	k (9−14 days)
$TiO_2-SiO_2-P_2O_5/CaO\_$ PVA	1.01	1.05	1.43
$TiO_2-SiO_2-P_2O_5/ZnO\_$ PVA	1.26	0.86	1.23
$TiO_2-SiO_2-P_2O_5/$ $CaO:TiO_2-SiO_2-P_2O_5/$ $ZnO\_$ PVA = 1:1	1.33	0.88	1.22
Tokem-250 _ PVA	1.20	0.16	0.41

Table 4. Level of Hemolysis for the Tested Samples

sample	level of hemolysis,%
$TiO_2-SiO_2-P_2O_5/CaO\_PVA$	0.72 ± 0.23
$TiO_2-SiO_2-P_2O_5/ZnO\_PVA$	28.07 ± 0.65
$TiO_2-SiO_2-P_2O_5/CaO:TiO_2-SiO_2-P_2O_5/ZnO\_PVA$ = 1:1	18.12 ± 0.27
Tokem-250 PVA	0.07 ± 0.44

insignificantly, and after 9 days, it was stabilized at pH 8.8. At the first stage, the pH increase created a favorable environment for crystallization of the calcium phosphate layer on the surface of the material.

The mechanism of apatite-like layer formation on the surface of the samples in the environment of the organism can be represented as a scheme (Figure 7).

The remaining of sodium ions after the incomplete ion exchange and the calcium ions in the inner layer were released, by exchanging with H_3O^+ ions into solution. Ti−OH/Si−OH groups were formed on the surface. The resulting Ti−OH/ (Si−OH) groups dissociated to form Ti−O-/Si−O-, which interacted with the positively charged Ca^{2+} ions in SBF. This leads to the formation of amorphous calcium titanate. As the calcium ions accumulated on the surface, the surface gradually acquired an overall positive charge. As a result, the positively charged surface combined with the negatively charged phosphate ions to form amorphous calcium phosphate.[30]

Figure 8 shows microphotographs and the distribution of elements on the surface of the samples after incubation in SBF solution.

According to the X-ray spectral analysis, it is clear that the samples were covered with an amorphous layer and the deposition of elements on the surface was uniform for all samples.

One of the key problems in biotissue engineering is the development of two- and three-dimensional matrices or scaffolds. The following biodegradable polymeric materials can be used: collagen, gelatin, and saturated α-hydroxy acid derivatives, including polymers of lactic and glycolic acids, sodium silicate (liquid glass), poly(vinyl alcohol), hyaluronic acid, aliphatic polyethers, etc. The choice of material depends on the functional purpose of the bioartificial tissue. In this study, poly(vinyl alcohol) was chosen as a binder to create a three-dimensional framework.

Four samples were immersed in a model SBF solution to determine the ability of zinc oxide and the binder to form a calcium-phosphate layer on the surface, i.e., (1) $TiO_2-SiO_2-P_2O_5/CaO\_PVA$; (2) $TiO_2-SiO_2-P_2O_5/ZnO\_PVA$; (3) $TiO_2-SiO_2-P_2O_5/CaO:TiO_2-SiO_2-P_2O_5/ZnO\_$ PVA= 1:1; and (4) Tokem-250_PVA. Figure 9 shows the curves of Ca^{2+} and Mg^{2+} ion accumulation on the surface. The graph shows that the deposition of ions occurs in three stages, in each stage the coefficient of accumulation of ions on the surface of the material was calculated and listed in Table 3.

It was found that the introduction of the binder slightly slowed down the formation of an apatite-like layer on the surface of the samples in the first stages. But after 9 days (stage 3) the coefficient of accumulation was greater for all samples with PVA. The mechanism of apatite-like layer formation on the surface of the samples did not change (Figure 7). On can conclude that PVA is a good binder.

3.6. Hemocompatibility of Samples. The hemolytic index for samples $TiO_2-SiO_2-P_2O_5/ZnO\_PVA$ and $TiO_2-SiO_2-P_2O_5/CaO:TiO_2-SiO_2-P_2O_5/ZnO\_PVA$ = 1:1 were found to be 28.07 ± 0.65% and 18.12 ± 0.27%, respectively, which represents the highest hemolysis levels in this sample (Table 4). At the same time, the hemolysis levels of the other samples were not different from the positive control ($p > 0.05$). No statistically significant differences were found directly between samples $TiO_2-SiO_2-P_2O_5/CaO\_PVA$ and Tokem-250_PVA.

It was found that the supernatant color intensity in the samples $TiO_2-SiO_2-P_2O_5/ZnO\_PVA$ and $TiO_2-SiO_2-P_2O_5/CaO:TiO_2-SiO_2-P_2O_5/ZnO\_PVA$= 1:1 exceeded the level of positive control. Consequently, these samples caused partial hemoglobin escape from erythrocytes into the supernatant. It was also found that the degree of hemolysis depended on the number of erythrocytes in the erythrocyte suspension. The most pronounced hemolysis was observed at a erythrocyte concentration of 1.0×10^9 erythrocytes/mL. Therefore, this concentration of erythrocytes was used in the further studies.

The method of cytocompatibility control tested in this work successfully proved to be a reliable express method of controlling the total cytotoxicity of materials. The investigated samples $TiO_2-SiO_2-P_2O_5/CaO\_PVA$ and Tokem-250_PVA did not exceed the permissible levels of hemolysis for medical materials in contact with blood according to GOST ISO 10993-4-2020.

4. CONCLUSIONS

In this study, the composite materials with spherical particle shape and core−shell structure were synthesized by a facile sol−gel method. The material framework was TiO_2−SiO_2−P_2O_5 with 65 mol % TiO_2, 30 mol % SiO_2, and 5 mol % P_2O_5. The inner part was filled with CaO (TiO_2−SiO_2−P_2O_5/CaO) or ZnO (TiO_2−SiO_2−P_2O_5/ZnO). The temperature regimes and stages of composite formation were determined in this study. A stepwise heat treatment (drying in a drying oven at 60 °C for 30 min, then annealing in a muffle furnace for 30 min at 150, 250, 350 °C, for 6 h at 600 °C, and for 1 h at 800 °C) was required to obtain a homogeneous material. The obtained composites were characterized by a regular structure and highly developed surface. The samples had high biological activity, as the surface contains active centers (Si^{4+}, Ti^{4+}) which contributed to mineralization and precipitation of the calcium-phosphate compounds on the surface from biological media. Poly(vinyl alcohol) was used as a binder to bind spherical particles together when introduced into the biosubstrate. The TiO_2−SiO_2−P_2O_5/CaO_PVA samples did not exceed acceptable hemolysis levels for medical materials, while the TiO_2−SiO_2−P_2O_5/ZnO_PVA and TiO_2−SiO_2−P_2O_5/CaO:TiO_2−SiO_2−P_2O_5/ZnO_PVA = 1:1 samples had overestimated positive control values.

■ AUTHOR INFORMATION

Corresponding Author

Yu-Wen Chen − *Department of Chemical and Materials Engineering, National Central University, Jhongli 32001, Taiwan;* ⊙ orcid.org/0000-0002-8519-2595; Phone: +886-34227151 ext. 34203; Email: ywchen@cc.ncu.edu.tw

Authors

Ekaterina S. Lyutova − *National Research Tomsk State University, Tomsk 634050, Russia*

Valeriya A. Tkachuk − *National Research Tomsk State University, Tomsk 634050, Russia*

Liliya A. Selyunina − *National Research Tomsk State University, Tomsk 634050, Russia*

Lyudmila P. Borilo − *National Research Tomsk State University, Tomsk 634050, Russia*

Dmitriy A. Fedorishin − *National Research Tomsk State University, Tomsk 634050, Russia*

Complete contact information is available at:
https://pubs.acs.org/10.1021/acsomega.2c05398

Notes

The authors declare no competing financial interest.

■ ACKNOWLEDGMENTS

■ REFERENCES

(1) Bommala, V. K.; Krishna, M. G.; Rao, C. T. Magnesium matrix composites for biomedical applications: a review. *J. Magnes. Alloy.* **2019**, *7*, 72−79.

(2) Munir, K.; Lin, J.; Wen, C.; Wright, P. F.; Li, Y. Mechanical, corrosion, and biocompatibility properties of Mg-Zr-Sr-Sc alloys for biodegradable implant applications. *Acta Biomater.* **2020**, *102*, 493−507.

(3) Yue, Y.; Xu, P.; Lei, Z.; Li, K.; Xu, J.; Wen, J.; Wang, S.; Cheng, W.; Lin, S.; Huang, Z.; Xu, H. Preparation and characterization of a novel drug-loaded Bi-layer scaffold for cartilage regeneration. *RSC Adv.* **2022**, *12*, 9524−9533.

(4) Relvas, C.; Reis, J.; Potes, J. A. C.; Fonseca, F. M. F.; Simoes, J. A. O. Rapid manufacturing system of orthopedic implants. *Revista Brasileira de Ortopedia (English Edition).* **2009**, *44*, 260−265.

(5) Muley, S. V.; Vidvans, A. N.; Chaudhari, G. P.; Udainiya, S. An assessment of ultra fine grained 316L stainless steel for implant applications. *Acta Biomater.* **2016**, *30*, 408−419.

(6) Niinomi, M.; Nakai, M.; Hieda, J. Development of new metallic alloys for biomedical applications. *Acta Biomater.* **2012**, *8*, 3888−3903.

(7) Asri, R. I. M.; Harun, W. S.W.; Samykano, M.; Lah, N. A. C.; Ghani, S. A. C.; Tarlochan, F.; Raza, M. R. Corrosion and surface modification on biocompatible metals: a review. *Mater. Sci. Eng. C* **2017**, *77*, 1261−1274.

(8) Minagar, S.; Berndt, C. C.; Wang, J.; Ivanova, E.; Wen, C. A review of the application of anodization for the fabrication of nanotubes on metal implant surfaces. *Acta Biomater.* **2012**, *8*, 2875−2888.

(9) Su, Y.; Cockerill, I.; Zheng, Y.; Tang, L.; Qin, Y.; Zhu, D. Biofunctionalization of metallic implants by calcium phosphate coatings. *Bioact. Mater.* **2019**, *4*, 196−206.

(10) Su, T.; Luo, C.; Zhang, Z.; Hermawan, H.; Zhu, D.; Huang, J.; Liang, Y.; Li, G.; Ren, L. Bioinspired surfacefunctionalization of metallic biomaterials. *J. Mech. Beh. Biomed.* **2018**, *77*, 90−105.

(11) Sola, A.; Bellucci, D.; Cannillo, V.; Cattini, A. Bioactive glass coatings: a review. *Surface Eng.* **2011**, *27*, 560−572.

(12) Al-Sanabani, J. S.; Madfa, A. A.; Al-Sanabani, F. A. Application of Calcium Phosphate Materials in Dentistry. *Int. J. Biomater.* **2013**, *2013*, 1−12.

(13) Jeong, J.; Kim, J. H.; Shim, J. H.; Hwang, N. S.; Heo, C. Y. Bioactive calcium phosphate materials and applications in bone regeneration. *Biomaterials Research.* **2019**, *23*, 87−96.

(14) Epple, M.; Ganesan, K.; Heumann, R.; Klesing, J.; Kovtun, A.; Neumann, S.; Sokolova, V. Application of calcium phosphate nanoparticles in biomedicine. *J. Mater. Chem.* **2010**, *20*, 18−23.

(15) Riehemann, K.; Schneider, S. W.; Luger, T. A.; Godin, B.; Ferrari, M.; Fuchs, H. Nanomedicine - challenge and perspectives. *Angew. Chem., Int. Ed. Engl.* **2009**, *48*, 872−897.

(16) Heimann, R. B.*Classic and Advanced Ceramics from Fundamentals to Application*; Wiley, 2010; p 573.

(17) Al-Sanabani, J. S.; Madfa, A. A.; Al-Sanamani, F. A. Application of Calcium Phosphate Materials in Dentistry. *Int. J. Biomater.* **2013**, *2013*, 876132.

(18) Maimaiti, B.; Zhang, N.; Yan, L.; Luo, J.; Xie, C.; Wang, Y.; Ma, C.; Ye, T. Stable ZnO-doped hydroxyapatite nanocoating for anti-infection and osteogenic on titanium. *Colloids Surf. B Biointerfaces.* **2020**, *186*, 110731.

(19) Jmal, N.; Bouaziz, J. Synthesis, characterization and bioactivity of a calcium-phosphate glass-ceramics obtained by the sol-gel processing method. *Mater. Sci. Eng., C* **2017**, *71*, 279−288.

(20) Teow, S. Y.; Wong, M. M.; Yap, H. Y.; Peh, S. C.; Shameli, K. Bactericidal properties of plants-derived metal and metal oxide nanoparticles (NPs). *Molecules.* **2018**, *23*, 1366−1375.

(21) Hanley, C.; Layne, J.; Punnoose, A.; et al. Preferential killing of cancer cells and activated human T cells using ZnO nanoparticles. *Nanotechnology.* **2008**, *19*, 295103.

(22) Khader, A.; Arinzeh, T. L. Biodegradable zinc oxide composite scaffolds promote osteochondral differentiation of mesenchymal stem cells. *Biotechnol. Bioeng.* **2020**, *117*, 194−209.

(23) Zhang, T.; Liu, J.; Fellner, M.; Zhang, C.; Sui, D.; Hu, J. Crystal structures of a ZIP zinc transporter reveal a binuclear metal center in the transport pathway. *Sci. Adv.* **2017**, No. 8, 1700344.

(24) Juhasz, J. A.; Best, S. M. Bioactive ceramics: Processing, structures and properties. *J. Mater. Sci.* **2012**, *47*, 610−624.

(25) Bose, S.; Tarafder, S. Calcium phosphate ceramic systems in growth factor and drug delivery for bone tissue engineering: a review. *Acta Biomater.* **2012**, *8*, 1401−1421.

(26) Kambe, T.; Tsuji, T.; Hashimoto, A.; Itsumura, N. The physiological, biochemical, and molecular roles of zinc transporters in zinc homeostasis and metabolism. *Physiol. Rev.* **2015**, *95*, 749−784.

(27) Li, Y.; Yang, Y.; Qing, Y.; Li, R.; Tang, X.; Guo, D.; Qin, Y. Enhancing ZnO-NP Antibacterial and Osteogenesis Properties in Orthopedic Applications: A Review. *Inter. J. Nanomed.* **2020**, *15*, 6247−6262.

(28) Yamaguchi, M. Role of nutritional zinc in the prevention of osteoporosis. *Mol. Cell. Biochem.* **2010**, *338*, 241−254.

(29) Huang, T.; Yan, G.; Guan, M. Zinc homeostasis in bone: zinc transporters and bone diseases. *Inter. J. Mol. Sci.* **2020**, *21*, 1236−1245.

(30) Letaïef, N.; Lucas-Girot, A.; Oudadesse, H.; Dorbez-Sridi, R.; Boullay, P. Investigation of the surfactant type effect on characteristics and bioactivity of new mesoporous bioactive glass in the ternary system SiO_2-CaO-P_2O_5: structural, textural and reactivity studies. *Acta Biomater.* **2014**, *195*, 102−111.

(31) Shamsutdinova, A. N.; Kozik, V. V. Obtaining and properties of thin films based on titanium, silicon and nickel oxides. *Chem. Sustainabl.* **2016**, *24*, 699−704.

(32) Yilmaz, E.; Soylak, M. Functionalized nanomaterials for sample preparation methods. *Handbook of Nanomaterials in Analytical Chemistry.* **2020**, 375−413.

(33) Kozik, V. V.; Borilo, L. P.; Lyutova, E. S. Synthesis and properties of bioactive spherical materials for the TiO_2-SiO_2/CaO system. *Russ. J. Appl. Chem.* **2022**, *95*, 21−27.

(34) Kozik, V. V.; Borilo, L. P.; Lyutova, E. S.; Chen, Y. W. Influence of composition and preparation conditions on the structure and properties of composite materials TiO_2-SiO_2/CaO with spherical particle shape based on Tokem-200 cationic exchange resins. *ACS Omega* **2021**, *6*, 21104−21112.